Journal of Cell Biology and Histology
Volume 7 | Issue 1
ISSN: 2638-082X

Research Article Open Access

Cellular Junctions and their Role in Early Stages of Lung Injury and Covid-19 Induced Fibrosis

Julián Wiegner, Michael Kasper, Mirko HH Schmidt, Kathrin Barth*

Institute of Anatomy, Medical Faculty "Carl Gustav Carus", Technical University of Dresden, Fiedlerstr. 42, 01307 Dresden, Germany

***Corresponding Author:** Kathrin Barth, Institute of Anatomy, Medical Faculty "Carl Gustav Carus", Technical University of Dresden, Fiedlerstr. 42, 01307 Dresden, Germany, Tel: +49 351 458 6076, Fax: +49 351 458 6303, E-mail: kathrin.barth@tu-dresden.de

Citation: Julián Wiegner, Michael Kasper, Mirko HH Schmidt, Kathrin Barth (2025) Cellular Junctions and their Role in Early Stages of Lung Injury and Covid-19-Induced Fibrosis, J Cell Biol Histol 7(1): 102

Received Date: June 05, 2025 **Accepted Date:** July 05, 2025 **Published Date:** July 09, 2025

Abstract

Pulmonary fibrosis is a multifactorial chronic progressive disease, caused by numerous biotic and abiotic agents, including SARS-CoV-2 infection. Damage of the alveolar epithelial barrier (formed by alveolar epithelial cells type I, consisting of tight and adherens junctions) has been described as a key mechanism of early fibrosis and therefore could be crucial for post-acute sequelae of COVID-19 as well. Integrity of adherens junctions is regulated by the intracellular plaque protein p120 catenin and is crucial for epithelial barrier regulation in epithelial-mesenchymal-transition-driven diseases like fibrogenesis and cancer progression. Abundance and expression of p120 catenin and regulator proteins of intercellular contacts (caveolin-1, P2X7R) were investigated in FFPE-specimen of COVID-19 affected lungs (acute vs. chronic) compared to control and interstitial lung disease of other cause (n = 6 each), followed by further investigation of p120 catenin in early lung injury models using profibrotic agents in culture of murine lung and human alveolar epithelial cell culture. p120 catenin was higher in chronic vs. acute COVID-19, suggesting a role in fibrotic development. The interacting proteins caveolin-1 and P2X7R were simultaneously decreased in COVID-19, indicating an involvement in early pathophysiology. In vitro experiments for early epithelial damage showed no changes in p120 catenin and its phospho-Y228 site in cell culture while in murine lung culture p120 catenin was reduced. Thus, affection and interaction of p120 catenin and caveolae associated proteins could be a potential mechanism in COVID-19-induced pulmonary fibrosis.

Keywords: p120 catenin; COVID-19; caveolin-1; P2X7R; pulmonary fibrosis

Abbreviations: AEC: alveolar epithelial cell; AJ: adherens junctions; ARDS: acute respiratory distress syndrome; B2M: β2-Microglobulin; BLM: bleomycin; cav-1: caveolin-1; FCS: fetal calf serum; IF: immunofluorescence; IHC: immunohistochemistry; IP: immunoperoxidase; ILD: interstitial lung disease; LEL: Lycopersicon esculentum (Tomato) Lectin; PCLS: precision-cut lung slices; PF: pulmonary fibrosis; ROI: region of interest; RT: room temperature; TBP: TATA box binding protein; TJ: tight junctions; WB: Western Blot

Introduction

Pulmonary fibrosis (PF) is a chronic progressive lung disease which is characterised by significant extracellular matrix (ECM) deposition, leading to interstitial expansion and capillary weakening, ultimately resulting in ventilatory failure [1–6]. Multiple abiotic and biotic factors are able to cause PF, including the Severe Acute Respiratory Syndrome Coronavirus 2 (SARS-CoV-2), the causative agent of the Coronavirus Disease 2019 (COVID-19) [7–10]. PF, one of the most concerning post-acute sequelae of COVID-19, typically manifests subsequent to acute lung injury, especially after acute respiratory distress syndrome (ARDS). ARDS represents a severe, acute form of microvascular lung injury (with the histopathologic finding of diffuse alveolar damage, DAD), characterised by an immediate exudative inflammatory and a proliferative phase associated with alveolar epithelial cell (AEC) hyperplasia [8, 11, 12]. It has been observed that COVID-19 patients are at high risk with development of ARDS in about 30 % of all COVID-19 cases [13] with following fibrotic changes in 7 % of all confirmed COVID-19 cases [14–16] as a result of abnormal tissue repair responses during chronic inflammatory and profibrotic conditions [7, 8, 17, 18].

An initial and ongoing damage of the alveolar epithelial barrier leads to cell differentiation (epithelial-mesenchymal transition, EMT) and increased production of profibrotic factors, which seems to be pivotal for fibrogenesis [1]. (Myo)fibroblasts are cells that play a crucial role in the processes of wound healing and the formation of connective tissue [19]. In COVID-19 and PF of other cause, fibroblasts are activated and contribute to the formation of excess connective tissue and drive disease progression [20]. The signalling pathways involved in COVID-19 and PF of other cause are intricate and interact with one another. Transforming growth factor beta (TGF-β), activated through inflammatory processes, plays a pivotal role in the pathogenesis of fibrosis [21]. TGF-β has been demonstrated to promote fibroblast activation and ECM production, which ultimately leads to scar tissue formation in the lungs [1, 22–24]. In order to gain insight into the underlying mechanisms of COVID-19 and PF in general, we concentrated our efforts on the damage to AECs.

The initial epithelial damage at disease onset is characterised by a loss of intercellular connections, which play a pivotal role in maintaining the barrier function of the alveolar epithelium [25–27]. The alveolar epithelium, mainly formed by AEC type I (AECI) [28], features three main types of intercellular connections: tight junctions (TJ), adherens junctions (AJ) and desmosomes [29]. Together with the TJ, the AJ are involved in the formation of the apicoadherent contacts, which serve to separate the apical and basolateral membranes from each other, thereby maintaining cell polarity and separation of the external environment from the subepithelial tissue [30].

AJ consist of the calcium-dependent transmembrane protein E-Cadherin, which connects neighbouring cells [31–33]. On its cytoplasmic domain, it interacts with proteins of the catenin family (p120 catenin, β-catenin, plakoglobin) [34,35]. The protein p120 catenin is an armadillo repeat domain containing protein, which interacts dynamically with E-Cadherin, regulating the integrity of AJ as well as enzyme activity of Rho GTPases [36–38], by which it is involved in EMT [39], a hallmark of fibrosis and tumor progression [40].

AJ are strongly associated with caveolae, invaginated specialized rafts, which contain proteins of the caveolin family and a specific lipid composition for signalling processes regulating the pathogenesis of tumor progression and PF [41–43]. Caveolin-1 (cav-1) is the best studied member of this protein family and is preferably expressed in AECI in the lung, interacting with several signalling pathways like TGF-β [44,45]. Changes in cav-1 expression are associated with altered epithelial morphology and changes in TJ and AJ protein abundance [46,47]. In AECI, the extracellular ATP gated cation channel P2X7R is also interacting with cav-1 [48,49] and has a central function in inflammatory and fibrotic diseases [50,51].

To investigate the involvement of the alveolar epithelium, cell-cell contacts (p120 catenin) and pro-fibrotic signalling pathways in pulmonary fibrogenesis, immunohistochemical studies were carried out retrospectively on COVID-19 impaired human lung

samples obtained from the Tumor and Normal Tissue Bank (TNTB) of the NCT/UCC/UKD. Acute COVID-19 courses were compared to chronic courses; further controls were a group with death of non-pulmonary cause and a group with an interstitial lung disease (ILD) of other origin (negative COVID-19 or pre-pandemic time of death). To clarify the role of p120 catenin and its phosphorylation status in pro-fibrotic development, early injury models of human alveolar epithelial cell line NCI-H441 and murine lung tissue culture were investigated using TGF-β and bleomycin (BLM), which is a widely used model for lung injury investigation due to its side effect of lung toxicity. The study aims to investigate quantitative changes in p120 catenin and the caveolae-associated proteins in COVID-19 impaired human lung tissue and in vitro injury models, clarifying the involvement of these pro-fibrotic pathways in early lung damage.

Methods

For detailed description of all experimental procedures, please refer to supplemental material.

Human Tissue Samples

Human lung tissue samples were provided by the Tumor and Normal Tissue Bank (TNTB) of the NCT/UCC/UKD at Institute of Pathology of the University Hospital Carl Gustav Carus Dresden at the Technical University of Dresden and used following the ethics vote of the Technical University of Dresden (BO-EK-175052020). Specimens were matched into groups primarily by histological features using formalin-fixed, paraffin-embedded (FFPE) slices [7,8,17,52]: acute COVID-19 (n = 6), chronic COVID-19 (n = 4), interstitial lung disease (ILD) of different origin (n = 6), and healthy lung (n = 6). See supplemental material for detailed information.

Animal Tissue Culture

Wildtype (WT) mice (n = 4) of the C57BL/6 strain were purchased from Charles River Laboratories. The mice were kept in the animal facility of the Medical Faculty Carl Gustav Carus, Technical University of Dresden with food and water ad libitum. The experimental procedures were approved by the state directorate Dresden (DD24-5131/365/19 and TVT17/2016).

Cell Culture

Human lung NCI-H441 cells [53–55] were cultivated in RPMI-1640 medium (ATCC), adding 10 % fetal calf serum (FCS) at 37 °C with 5 % CO_2. For experimental conditions, culture medium was enriched with ITS (insulin, transferrin, selenous acid) and dexamethasone [55,56], 100 mU/ml BLM (STADApharm GmbH) or 1 ng/mL TGF-β (R&D Systems) were added. For immunostaining, NCI-H441 cells were seeded on poly-lysine coated cover slips [57]. After treatment, cells were fixed with an acetone-methanol solution and stored at -20 °C.

Western Blot (WB) Analysis

Protein concentration of lysed NCI-H441 cells was determined using the Pierce™ bicinchoninic acid (BCA) Protein Assay Kit (Pierce Biotechnology). 20 µg of sample protein were transferred into 4x LI-COR® loading buffer, heat-denatured, separated in a 10 % SDS-polyacrylamide gel and transferred on an Immobilon®-FL polyvinylidene difluoride (PVDF) membrane (Merck Millipore).

The total protein was stained with the Revert™ 700 Total Protein Stain Kit and detected on the Odyssey® Fc Imager. After destaining, the membrane was blocked with Intercept® (TBS) Blocking Buffer, incubated with the primary (Table 1) and secondary antibody (IRDye® 680 goat anti-mouse, IRDye® 800 goat anti-rabbit). Semi-quantitative analysis was done using Image Studio™ Lite (all from LI-COR Biosciences).

Table 1: Primary antibodies used for Western Blot, immunohistochemistry and immunofluorescence

Antibody	Dilution used		Host	Type	Supplier
	WB	IHC/IF			
anti-Caveolin 1 (D46G3) product no.: #3267	-	1:160	rabbit	monoclonal	Cell Signaling Technology (Danvers (MA), USA)
anti-p120 catenin (6H11) product no.: 33-9700	1:500	1:8.000 (PCLS - IHC) 1:800 (PCLS - IF) 1:20 (human)	mouse	monoclonal	Invitrogen (Carlsbad (CA), USA)
anti-p120 catenin phospho-Y228 product no.: PA5-40286	1:500	1:1.000 (PCLS - IHC) 1:100 (PCLS - IF)	rabbit	polyclonal	Invitrogen (Carlsbad (CA), USA)
anti-p120 catenin phospho-Y228 product no.: C358960	-	1:20 (human)	rabbit	polyclonal	LifeSpan BioSciences, Inc. (Seattle (WA), USA)
Anti-P2X7R product no.: 177 003	-	1:40	rabbit	polyclonal	Synaptic Systems (Göttingen)

mRNA Quantification Using Real-Time Reverse Transcription PCR (Real-time RT-PCR)

For extraction of mRNA, protein and DNA lysis, human FFPE slices were processed using the NucleoSpin® totalRNA FFPE XS Kit (Macherey-Nagel GmbH & Co. KG). For cDNA synthesis, RevertAid H Minus 1st Strand Synthesis Kit (Thermo Fisher Scientific Inc.) was utilized, applying the Techne TC-512 Thermal Cycler (Keison Products). SsoAdvanced™ Universal Inhibitor--Tolerant SYBR® Green Supermix was used for qPCR on the CFX96 Touch Real-Time PCR Detection System (both from Bio-Rad Laboratories GmbH) (for primers see Table 2). The relative mRNA expression was calculated with the $\Delta\Delta C_t$ method using β2-Microglobulin (*B2M*) and TATA box binding protein (*TBP*) as housekeeping genes.

Table 2: Primer sequences for RT-PCR

Gene	NCBI n.o.	Sequence	Length
huB2M	AF072097.1	5'-GGTTTCATCCATCCGACATTG-3' 5'-GGTTCACACGGCAGGCATAC-3'	166 bp
huCAV1	BT007143.1	5'-AACCGCGACCCTAAACACCT-3' 5'-CCTTCCAAATGCCGTCAAAA-3'	103 bp
huCTNND1	BC075795.1	5'-GCCTCTGCCCTGGATTGGTT-3' 5'-ATGGAAGGGCGGGAGGAGAT-3'	144 bp
huP2RX7	BC007679.2	5'-AGTCACTCGGATCCAGAGCATGA-3' 5'-CACTCACCAGAGCAAAGCAAACG-3'	92 bp
huTBP	BT019657.1	5'-CGGTTTGCTGCGGTAATCAT-3' 5'-GGCTCCTGTGCACACCATTT-3'	87 bp

Culture and Paraffin Embedding of Precision-Cut Lung Slices (PCLS)

PCLS were generated as described previously [58–60] with slight alterations. Briefly, WT mice were euthanized, exsanguinated and the lungs were perfused with 0.8 % agarose. After isolation, the lungs were embedded in 3 % agarose and sliced into 500 µm thick PCLS. After treatment with 300 mU/mL BLM in DMEM/F12 medium, PCLS were fixed with 4 % formalin, incubated in 0.1 M Sørensen buffer, an ascending ethanol series, xylene and paraffin, followed by final embedding.

Immunohistochemistry (IHC) Using Immunoperoxidase (IP) and Immunofluorescence (IF)

For immunohistochemical staining of the human and murine PCLS, 5 µm paraffin slices were dewaxed and rehydrated by incubation in xylene, a descending ethanol series and water.

IP staining of the PCLS of murine lung was performed as previously described [59] using the VECTASTAIN® Elite® ABC Kit (Vector Laboratories). Antigen retrieval was performed in sodium citrate buffer. The slices were treated with 0.3 % hydrogen peroxide solution, blocked with 1.5 % normal serum, followed by incubation with the primary antibody (Table 1) and secondary antibody. Afterwards they were incubated with the VECTASTAIN ABC Reagent and stained 3,3'-diaminobenzidine (DAB) incubation. Counterstaining was done with Mayer's hemalum solution. The slides were washed in tap water, dehydrated using an ascending ethanol series and xylene, followed by embedding with DePeX.

IF experiments on the murine PCLS were done with additional lectin staining with Lycopersicon esculentum (Tomato) Lectin (LEL), biotinylated, 1:1.600 and secondary antibody incubation with Texas Red® Avidin D, 1:400 (both from Vector Laboratories) [61]. After final staining with DAPI Nucleic Acid Stain (Invitrogen) the slides were embedded with Fluoromount-G™ (Life Technologies Corp.).

For IF staining of the human NCI-H441 cells, cover slips were defrosted, followed by blocking with 1 % BSA. The human lung slices were additionally bleached in 6 % H_2O_2 for 10 min after rehydrating and afterwards demasked using EDTA buffer. The following steps were performed as described for murine PCLS.

IF stained specimen were detected using the Leica DM6 B fluorescence microscope (Leica Microsystems GmbH). Analysation was performed afterwards in (Fiji is Just) ImageJ (U. S. National Institutes of Health). For comparison of signal intensity, mean fluorescence intensity (MFI) was measured using a protocol previously described by Shihan et al. [62]. For definition of the region of interest (ROI), see supplemental material.

Statistical Analysis

Each data set was checked for normal distribution using Shapiro-Wilk test. For significance testing of normally distributed data, a two-tailed paired Student's t-test for two groups or one-way ANOVA for more groups was performed, followed by a Bonferroni post-hoc test. If not normally distributed, a Wilcoxon signed-rank test for two groups or ANOVA (Friedman test for paired groups and Kruskal-Wallis test for unpaired groups, followed by Dunn's post-hoc test) for more than two groups was used. The software GraphPad Prism was used for calculating. Significance levels were defined as * $p \leq 0.05$ and ** $p \leq 0.01$.

Results

p120 Catenin Increases In Chronic COVID-19

Since p120 catenin regulates AJ integrity and fibrotic changes through Rho GTPases activity [36–38,40], changes of p120 catenin were investigated in human lung.

Using IF staining, p120 catenin was shown to be localised in the cell membrane of AECI but also accumulated in aggregates in AECII (Figure 1A-H). p120 Catenin pan protein decreased in acute stage of COVID-19 compared to control (86.3 %) but increased significantly in chronic compared to acute stage (107.4 % vs. 86.3 %, $p = 0.0354$), while pY228 portion stayed at a low level (90.4 % in acute course, 92.3 % in chronic course). There was no statistically significant difference in pan protein between COVID-19 acute and ILD group (95.3 %), while pY228 portion increased significantly compared to acute stage COVID-19 (90.4 % vs. 115.1 %, $p = 0.0071$, Figure 1I).

The chronic COVID-19 group showed higher p120 catenin pan protein abundance than the acute course of the disease.

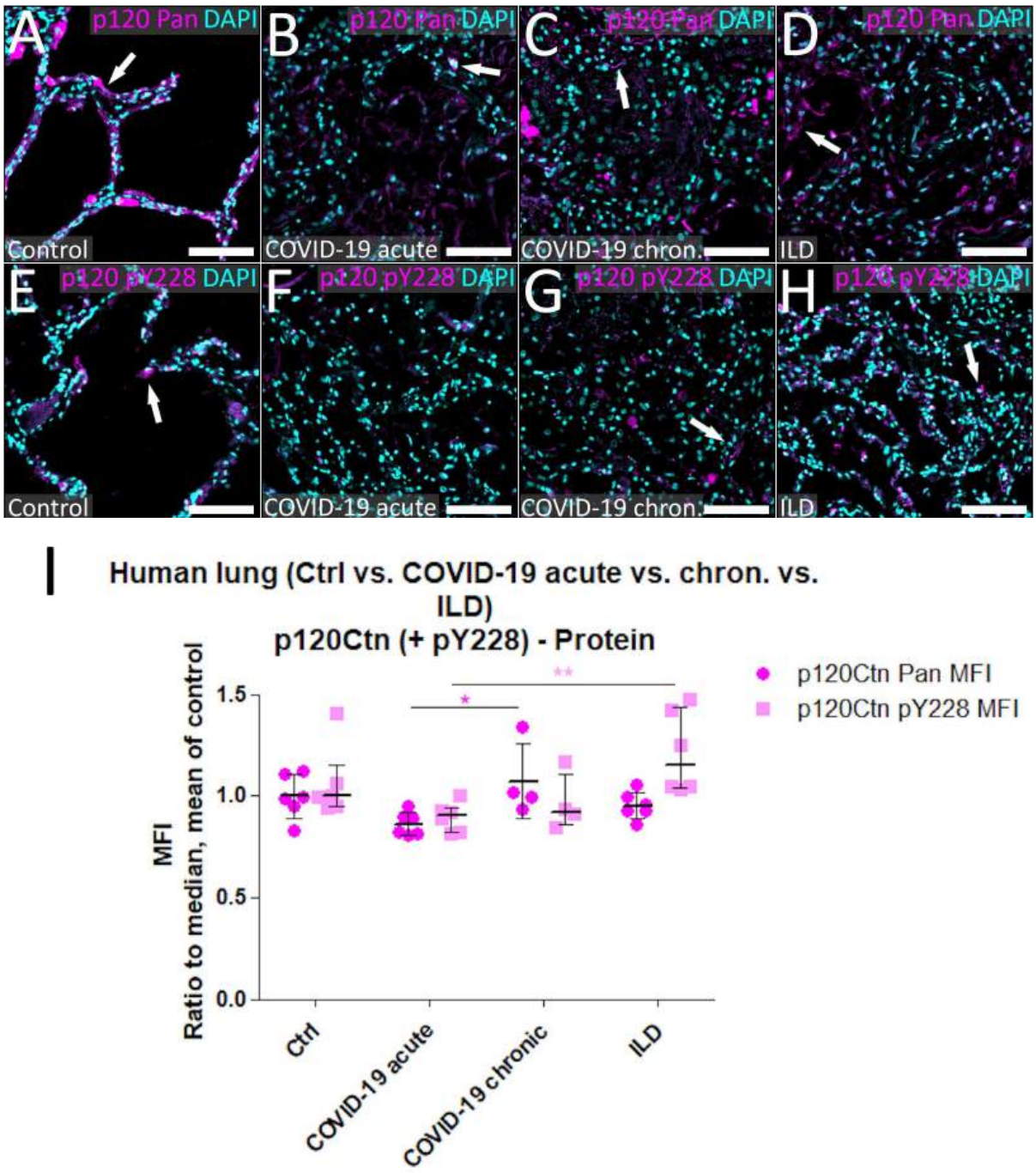

Figure 1: p120 Catenin protein abundance is increased in chronic COVID-19 compared to acute stage

A-H Retrospective human lung tissue of control (A, E), COVID-19 (acute, B, F), COVID-19 (chronic, C, G) and interstitial lung disease (ILD, D, H) of different origin were stained using indirect IF technique, p120 catenin pan (A-D) and pY228 (E-H) (magenta), DAPI nucleic stain (cyan). Representative pictures are shown. Arrows indicate p120 catenin signal in cell membrane of AECs. I Quantitative data of MFI of control (n = 6), COVID-19 acute (n = 6), COVID-19 chronic (n = 4) and ILD (n = 6) are shown as part of control mean (pan: mean ± SD ($p = 0.0354$), pY228: median ± IQR ($p = 0.0071$)). *$p < 0.05$, **$p < 0.01$. Scale bars = 100 µm (A-H).

Cav-1 and P2X7R Decrease in Acute Stage COVID-19

The AECI-specific proteins Cav-1 and P2X7R play a pivotal role in PF [44,45,50,63–66] and were therefore investigated in COVID-19 impaired human lung.

IF staining showed the localisation of cav-1 in the cell membrane of AECI forming some aggregates (Figure 2A-D). A significant decrease of cav-1 MFI in acute COVID-19 to 66.5 % ($p = 0.0226$) compared to control group was discovered, which was also demonstrated in mRNA expression (71.4 %, $p = 0.4351$). In chronic COVID-19, the difference to control in protein abundance was smaller (81.6 %) while expression decreased beyond that of the acute stage (48.8 %). In interstitial lung disease of different origin, abundance (74 %) and expression (80.8 %) of cav-1 protein were decreasing compared to control (Figure 2E).

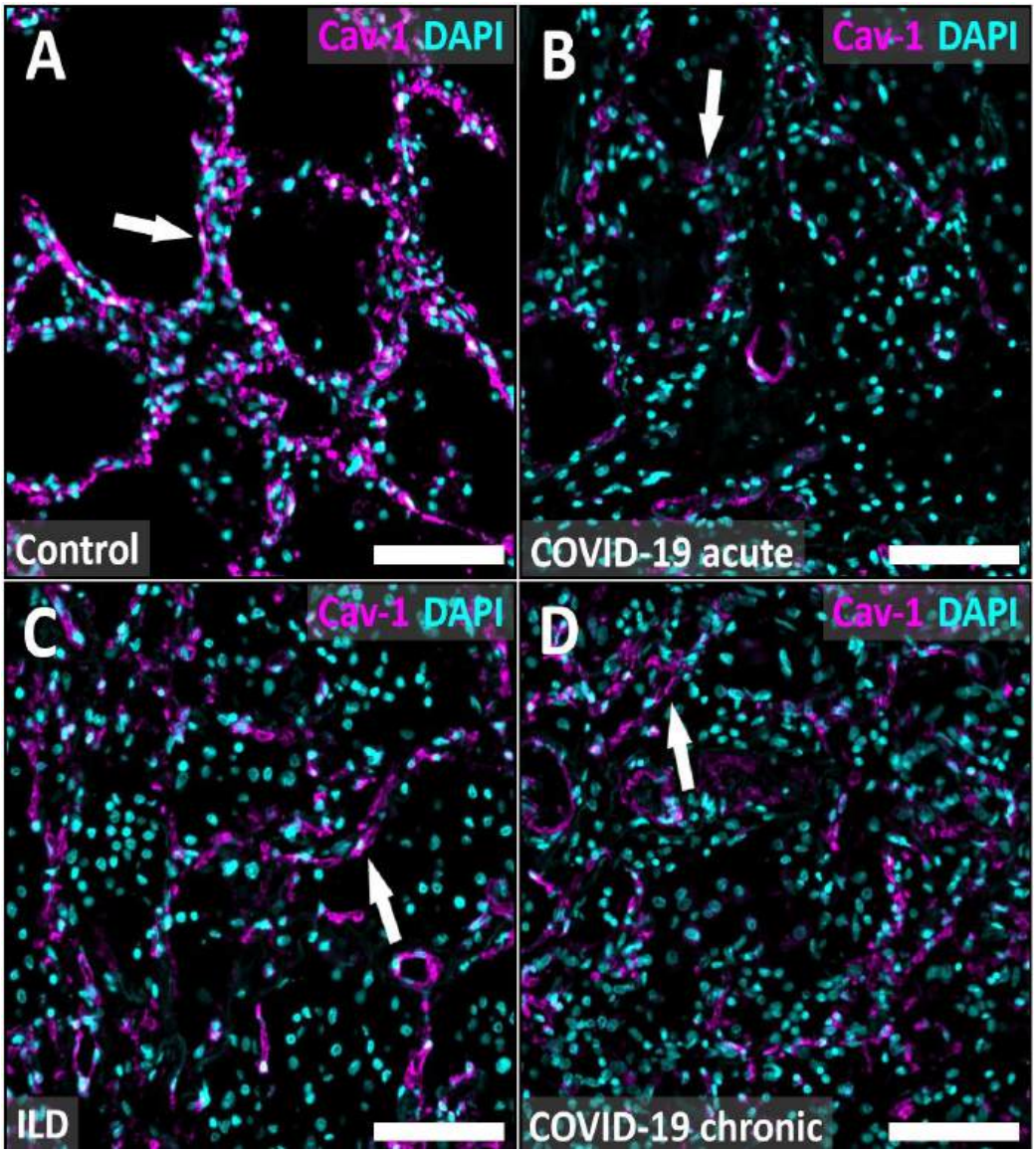

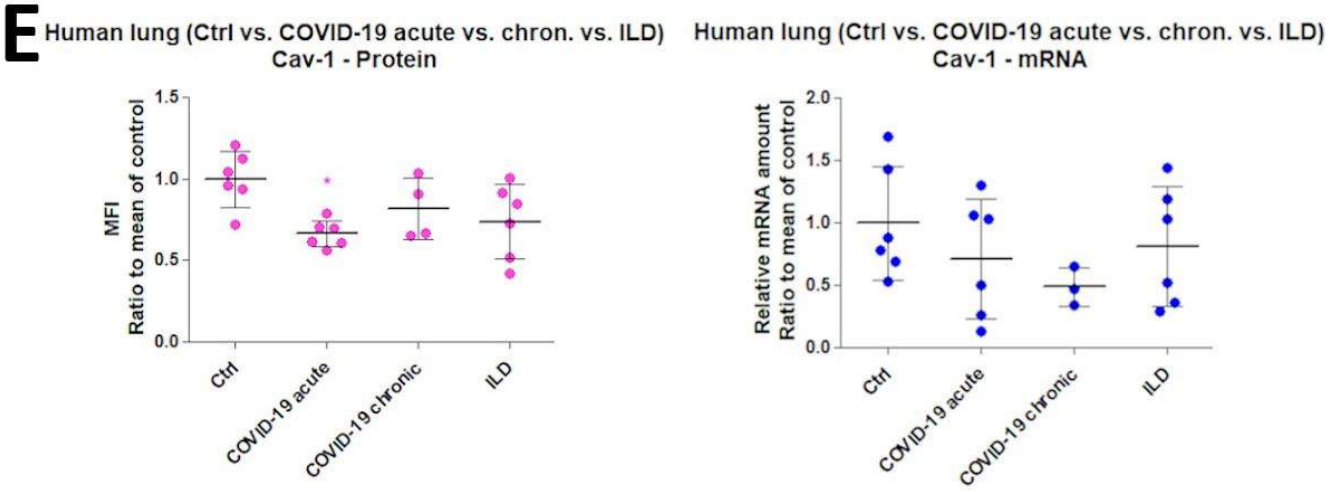

Figure 2: Cav-1 protein abundance and expression are decreased in the acute stage COVID-19 compared to control

P2X7R was shown to be localised in linear distribution as a cell membrane protein in the AECI (Figure 3A-D). Protein abundance of P2X7R was significantly decreased in acute COVID-19 (73.2 %, p = 0.0044) and in ILD (77.5 %) compared to control,a smaller decrease in chronic stage was seen (81.4 %). In contrast, mRNA expression of P2X7R was increased in groups ofCOVID-19 lung tissue (191 % in acute stage, 467 % in chronic stage, p = 0.1999, Figure 3E).

Both proteins, P2X7R and cav-1 were lower abundant in acute course of COVID-19.

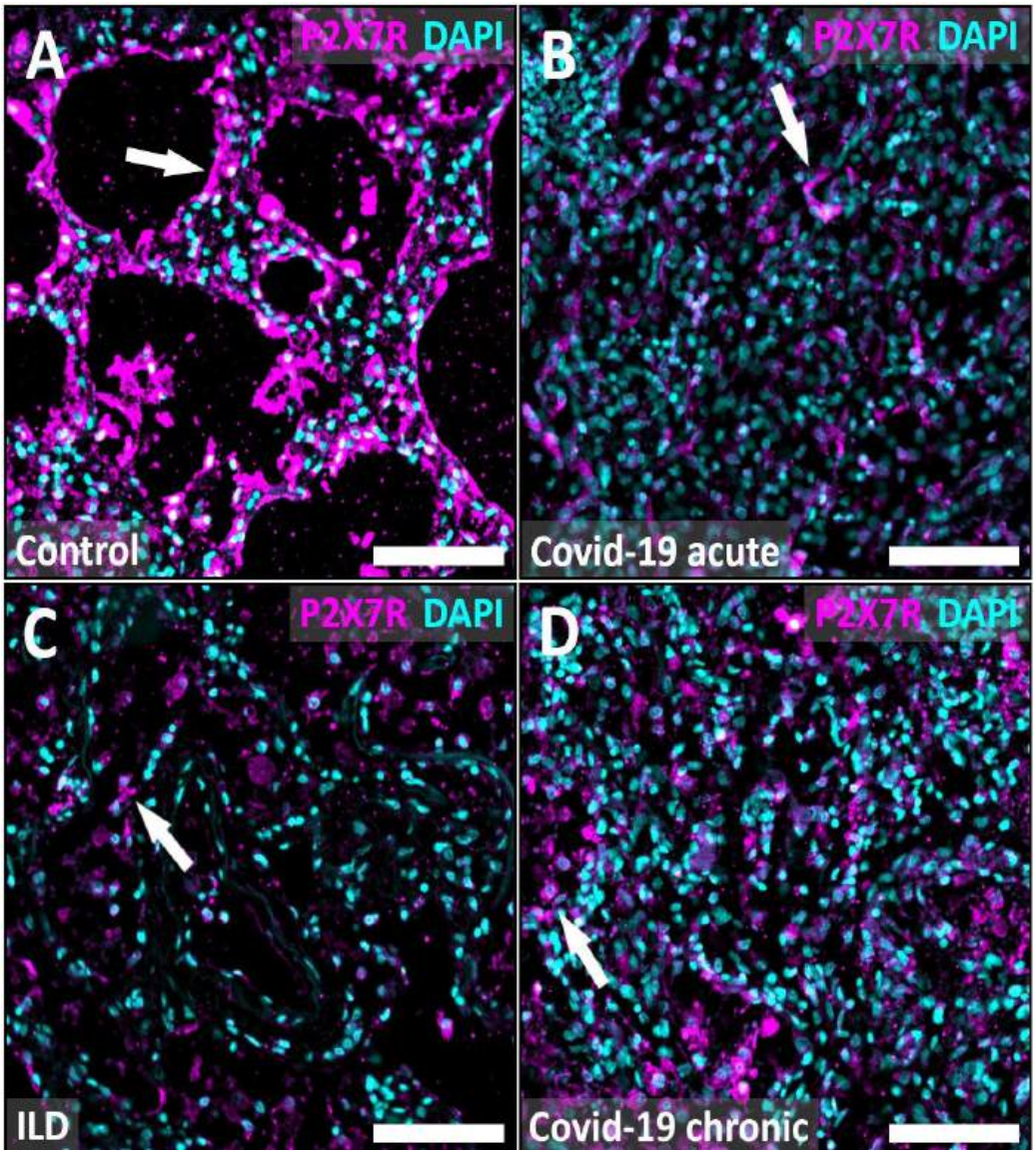

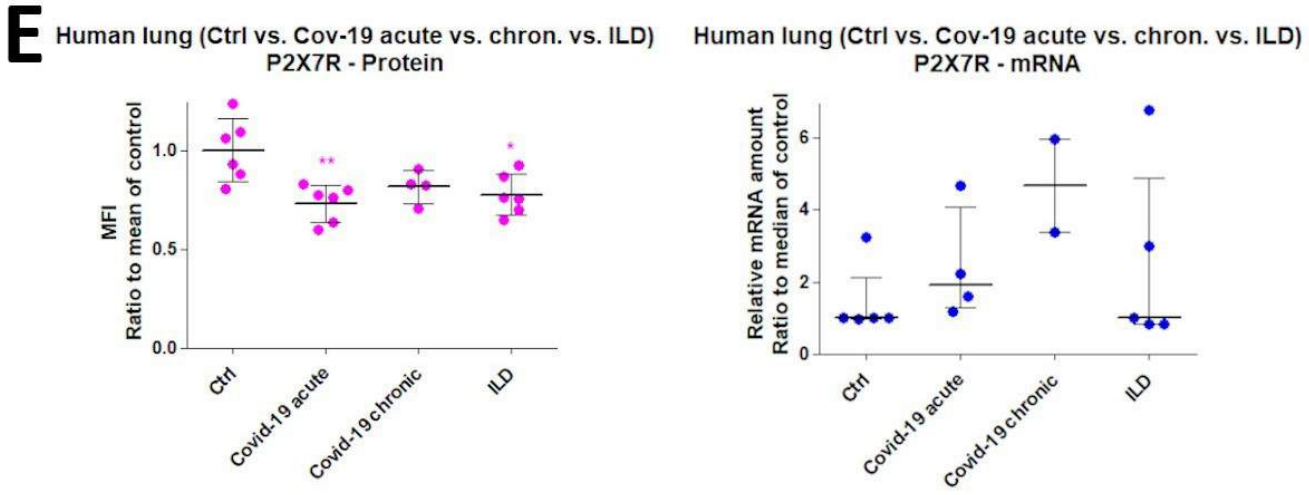

Figure 3: P2X7R protein abundance is decreased in COVID-19 acute, but not in chronic stage, while expression increases

A-D Retrospective human lung tissue of control (A), COVID-19 (acute, B), COVID-19 (chronic, D) and interstitial lung dis-ease (ILD, C) of different origin were stained using indirect IF technique, cav-1 (magenta), DAPI nucleic stain (cyan). Represen-tative pictures are shown. Arrows indicate cav-1 signal in cell membrane of AECs. E Quantitative data of MFI and mRNA lev-els normalized against house-keeping proteins TBP and B2M of control (n = 6 ; 6), COVID-19 acute (n = 6 ; 6), COVID-19chronic (n = 4 ; 3) and ILD (n = 6 ; 6) is shown as part of control mean (mean ± SD, MFI: p = 0.0226, mRNA: p = 0.4351). *p <0.05. Scale bars = 100 μm (A-D).

p120 Catenin pY228 Fraction Increases Time Dependently in BLM- and TGF-β-treated NCI-H441 Cells

To determine the influence of profibrotic factors on p120 catenin in early injury models of the alveolar epithelium, human NCI-H441 cells, as a model of a single cell type monolayer, were treated with BLM and TGF-β.

There were only slight, but not statistically significant changes in amount of p120 catenin pan protein (103.7% in 24 h BLM (p = 0.4134), 92.2 % in 48 h BLM (p = 0.2097), 99.5 % in 24h TGF-β (p = 0.9531), 103.8 % in 48 h TGFβ (p = 0.6859), Figure 4A). The pY228 fraction of p120 catenin pan protein amount showed a time dependent trend towards an increase in BLM- (96 % in 24 h (p = 0.36) vs. 117.7 % in 48 h (p = 0.0893)) and TGF-β (105.6 % in 24 h (p = 0.3565) vs. 122.5 % in 48 h (p = 0.1068)) treated NCI-H441 cells (Figure 4B).

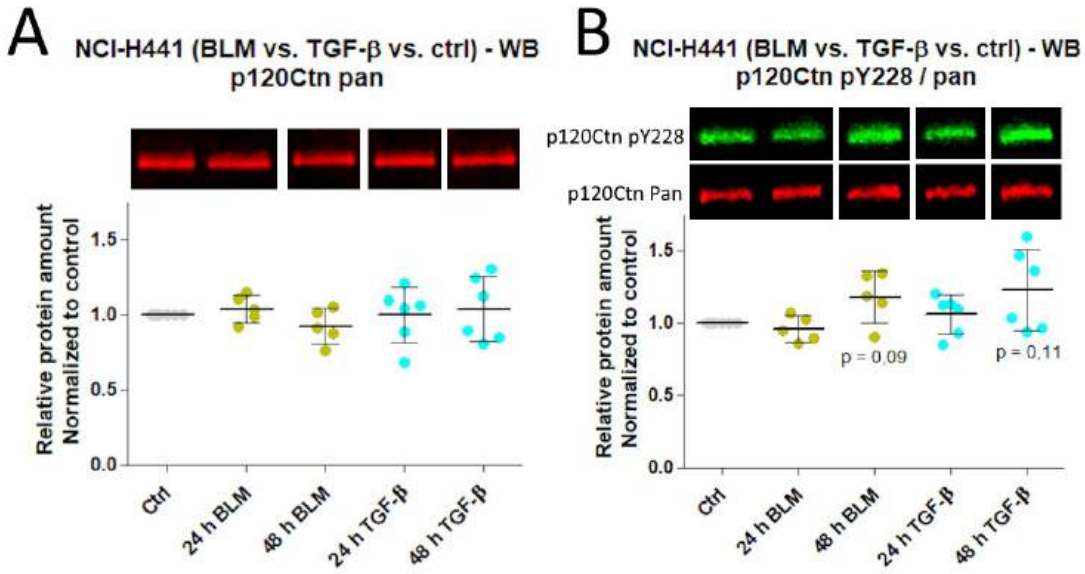

Figure 4: p120 catenin pan protein amount does not change in BLM- and TGF-β-treated NCI-H441 cells compared to control,

while p120 catenin pY228 fraction increases time dependently

A-B NCI-H441 cells were cultured and incubated with 100 mU/ml BLM or 1 ng/ml TGF-β for 24 h and 48 h compared to con-trol cells. Afterwards they were lysed, whole cell lysates were separated through gel electrophoresis and detected using WB tech-nique. Representative blots are shown. Band intensity was normalized to total protein staining of each lane (A) or to p120catenin pan protein (B). Quantitative data of normalized protein amount of control and BLM- (n = 5, pan 24 h: p = 0.4134, 48h: p = 0.2097, pY228 24 h: p = 0.36, 48 h: p = 0.0893) and TGF-β-treated (n = 6, pan 24 h: p = 0.9531, 48 h: p = 0.6859, pY22824 h: p = 0.3565, 48 h: p = 0.1068) NCI-H441 cells is shown as part of control mean (mean ± SD).

To further elucidate, if the p120 catenin amount, which is localized in the cell membrane, changes, fixed human NCI-H441 cells were double immunolabeled against the protein of interest and LEL. The staining showed p120 catenin mainly in the cell membrane with slight aggregates in the cytoplasm (Figure 5A-J).

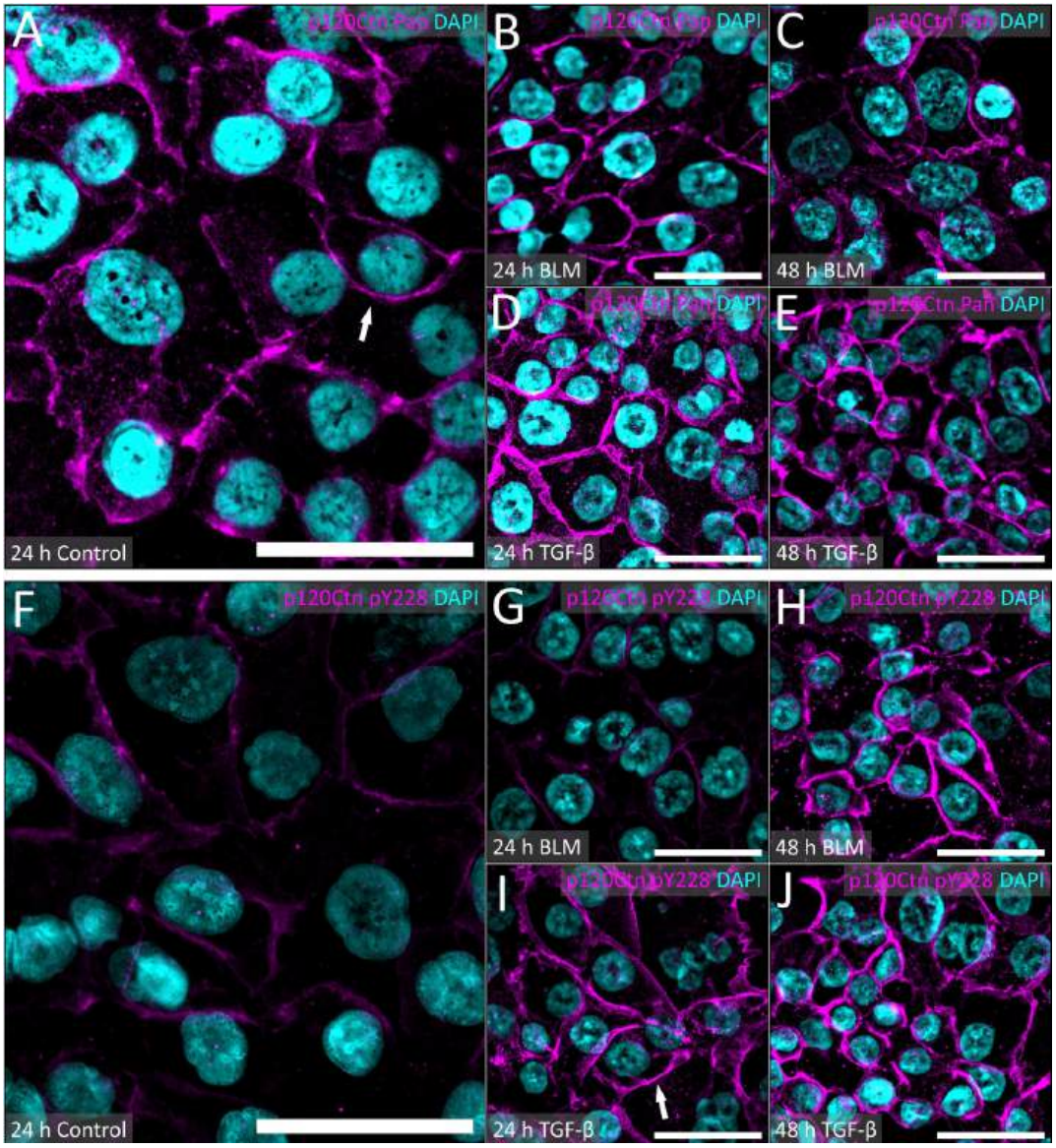

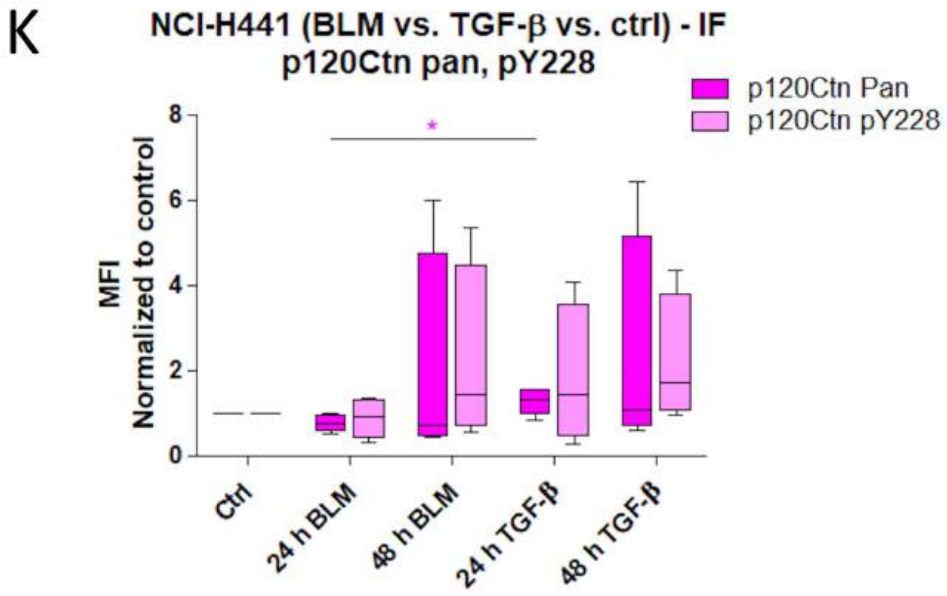

Figure 5: p120 catenin pan protein and pY228 show no changes in cell membrane abundance

A-J NCI-H441 cells were cultured and incubated with 100 mU/ml BLM or 1 ng/ml TGF-β for 24 h and 48 h compared to con-trol cells. Afterwards they were fixed and stained using indirect IF technique, p120 catenin pan (A-E) and pY228 (F-J) (magen-ta), DAPI nucleic stain (cyan). Representative pictures are shown. Arrows show p120 catenin in cell membrane. K Quantitativedata of MFI of control and BLM- (pan 24 h: $p = 0.1067$, 48 h: $p = 0.875$, pY228 24 h: $p = 0.6834$, 48 h: $p = 0.3458$) and TGF-β-treated (pan 24 h: $p = 0.1795$, 48 h: $p = 0.413$, pY228 24 h: $p = 0.3994$, 48 h: $p = 0.2183$) NCI-H441 cells ($n = 4$, pan 24 h BLMvs. TGF-β: $p = 0.0276$) is shown as part of control mean (box-and-whisker-plot). *$p < 0.05$. Scale bars = 50 µm (A-J).

MFI calculation was done in a defined ROI of lectin-stained area minus DAPI area for exclusive cell membrane measurements. p120 catenin pan protein abundance showed no significant changes in BLM (76.9 % in 24 h ($p = 0.1067$), 73.3 % in 48 h ($p = 0.875$)) and TGF-β (133.9 % in 24 h ($p = 0.1795$), 109.9 % in 48 h ($p = 0.413$)) treated human NCI-H441 cells in the cell membrane area, however the results were quite scattered. Human NCI-H441 cells treated with TGF-β for 24 h showed a significantly higher p120 catenin protein abundance than BLM-treated cells (133.9 % vs. 76.9 %, $p = 0.0276$). Comparable changes were seen in p120 catenin pY228 protein abundance (91.9 % in 24 h BLM ($p = 0.6834$), 146.1% in 48 h BLM ($p = 0.3458$), 144.3 % in 24 h TGF-β ($p = 0.3994$), 172.2 % in 48 h TGF-β ($p = 0.2183$), Figure 5K).

While p120 pan showed no relevant changes in whole cell lysates and cell membrane abundance, a small increment in the pY228 portion was seen in WB analysis, although not in the cell membrane.

p120 Catenin Decreases in BLM-treated Murine PCLS

To investigate the impact of a profibrotic milieu on changes of p120 catenin in a 3D model of early injured alveolar tissue excluding humoral factors, murine PCLS were treated with BLM.

IHC demonstrated p120 catenin localisation in the cell membrane of AECI and AECII with some abundance in the cytoplasm of AECII (Figure 6A-L).

p120 catenin protein abundance (MFI) increased in 24 h BLM-treated murine PCLS (144 %, $p = 0.4507$), but decreased significantly in 48 h treated murine PCLS compared to control (80.1 %, $p = 0.0291$). No changes in p120 catenin pY228 protein abundance were detected in murine PCLS (102.4 % in 24 h ($p = 0.8221$), 91.4 % in 48 h ($p = 0.4957$), Figure 6M).

So, in murine lung tissue excluding humoral factors p120 pan protein was downregulated through BLM-treatment.

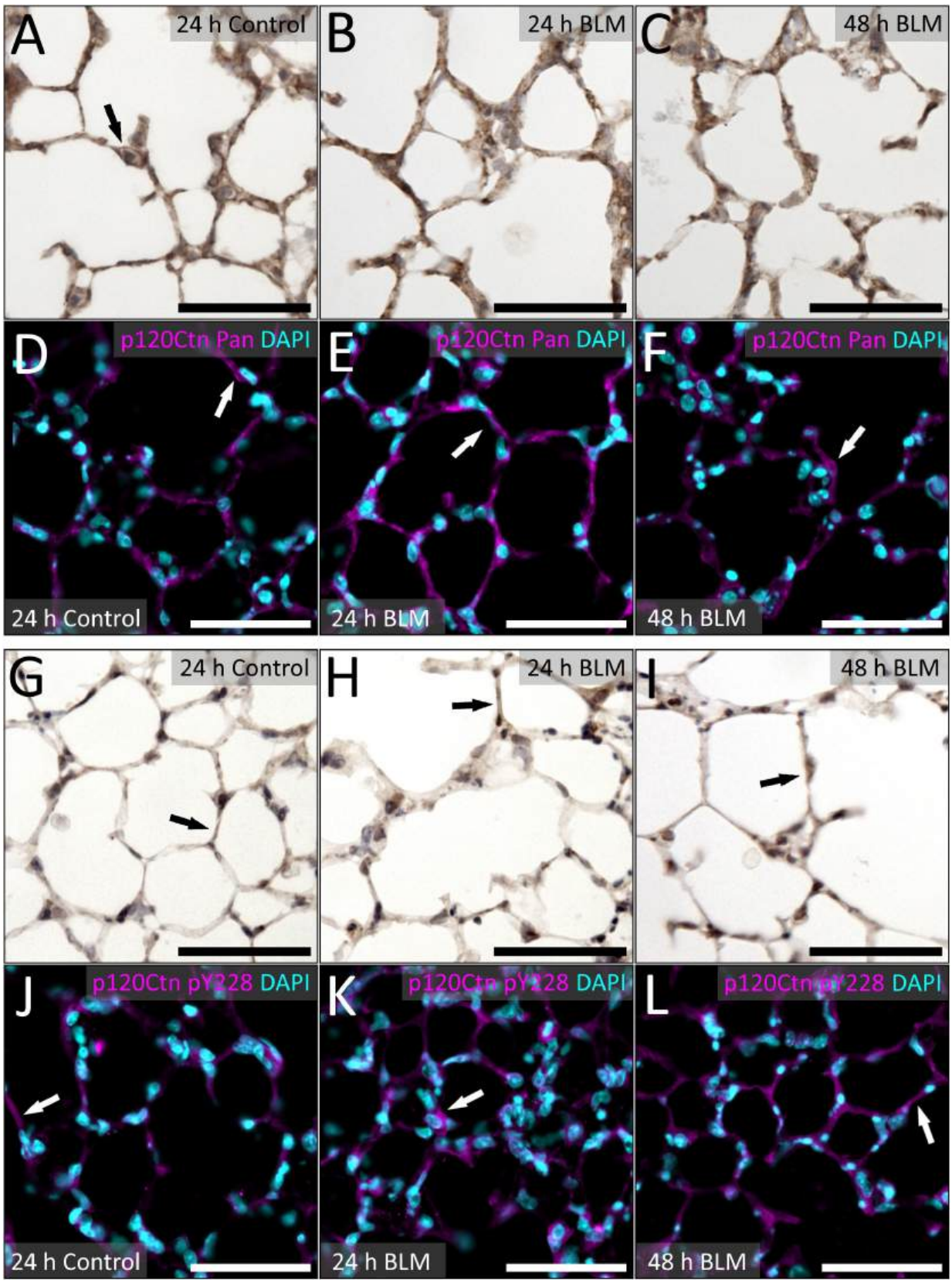
A
24 h Control
B
24 h BLM
C
48 h BLM
D
p120Ctn Pan DAPI
24 h Control
E
p120Ctn Pan DAPI
24 h BLM
F
p120Ctn Pan DAPI
48 h BLM
G
24 h Control
H
24 h BLM
I
48 h BLM
J
p120Ctn pY228 DAPI
24 h Control
K
p120Ctn pY228 DAPI
24 h BLM
L
p120Ctn pY228 DAPI
48 h BLM

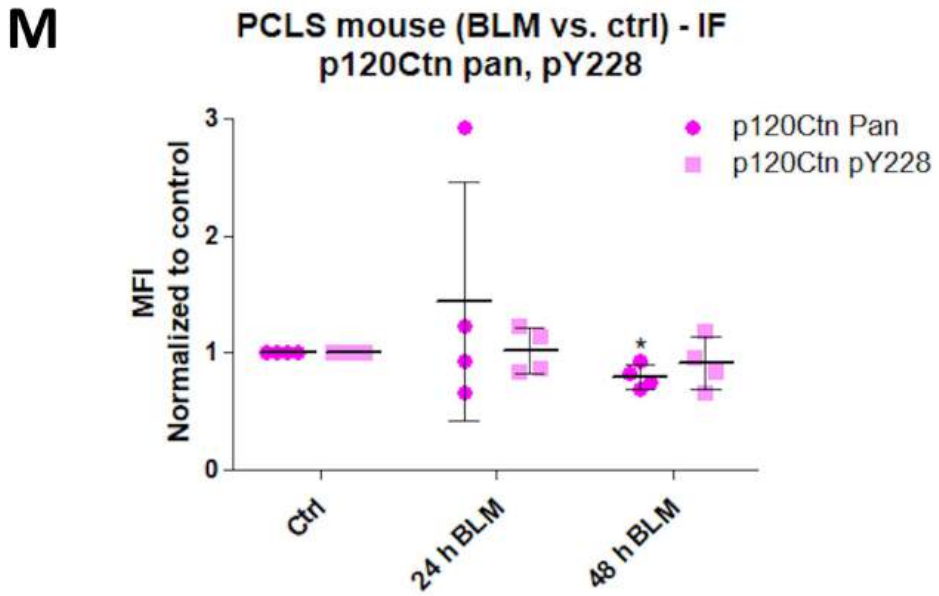

Figure 6: p120 catenin protein abundance decreases in 48 h BLM-treated murine PCLS compared to control

A-L PCLS of murine lung were freshly isolated, cultured and treated with 300 mU/ml BLM for 24 h and 48 h compared to un-treated control slices. Afterwards they were stained using IP (A-C, G-I) and indirect IF technique (D-F, J-L), p120 catenin pan(A-F) and pY228 (G-L) (magenta), DAPI nucleic stain (cyan). Representative pictures are shown. Arrows show p120 catenin inAECs. M Quantitative data of MFI of control and BLM-treated murine PCLS (n = 4) is shown as part of control mean (mean ±SD, pan 24 h: $p = 0.4507$, 48 h: $p = 0.0291$, pY228 24 h: $p = 0.8221$, 48 h: $p = 0.4957$). *$p < 0.05$. Scale bars = 50 µm (A-L).

Discussion

PF is a chronic, multifactorial disease, leading to progressive ventilatory failure. Nonetheless, pathways of disease development are not fully understood yet. Histologic similarities between COVID-19 lungs and interstitial lung diseases of other origins, e.g. (myo)fibroblast proliferation and activation [1,8,67–69] driven by pro-fibrotic pathways, such as TGF-β signalling [24,70,71] indicate common pathogenetic processes.

An early and ongoing epithelial damage of the alveolar epithelium seems to be crucial for the pathogenesis of PF [12,69]. The epithelial AJs are essential for maintaining barrier function and signal transduction [72]. Critical expression level of p120 catenin is one of the key regulatory proteins of AJ integrity by interaction with E-Cadherin [36,39,73,74]. Several phosphorylations of p120 regulate its binding capacity to E-Cadherin and the dissociation into the cytoplasm inducing downstream signalling pathways [37].

Investigating the protein in COVID-19, p120 catenin showed a significantly higher protein abundance in chronic COVID-19 compared to acute disease, indicating that upregulation of p120 could be one mechanism in fibrogenesis in COVID-19. It has been shown previously that p120 gets upregulated in profibrotic stages using TGF-β or BLM via transcriptional activity of SMAD and NF-κB pathways, blocking p120 expression attenuated fibroblast differentiation and pulmonary fibrosis [75].

The phosphorylated form p120 catenin pY228 was more abundant in ILD group compared to acute course of COVID-19. Phosphorylation of p120 at site Y228 is known to decrease the binding capacity to E-Cadherin while increasing binding to RhoA [76,77]. Increasing abundance of p120 catenin pY228 is associated with diverging tumor behavior [76,78]. Activity of Rho GTPases is crucial for processes of EMT: RhoA induces the formation of actin stress fibers, Rac1 and Cdc42 prompt the arrangement of podia, both leading to dissociation of epithelial cell contacts and increased migration [79,80]. A potential contribution of this specific phosphorylation to PF can still not be excluded.

Further investigations on p120 catenin and its pY228 form were done in human NCI-H441 cells using BLM and TGF-β. BLM is an antineoplastic drug, which is used for lymphoma and germ cell tumor treatment and has the common side effect of lung toxicity, possibly leading to PF, therefore being an established model for lung injury in early stages of lung fibrogenesis [81,82]. TGF-β is known as one of the main contributing cytokines driving PF [70]. WB of whole cell lysates treated with BLM or TGF-β for 24 h or 48 h revealed no relevant changes in the pan protein, while the pY228 fraction showed a small time-dependent increase, although not statistically significant. Quantifying the protein abundance in the cell membrane using MFI showed a time-dependent trend towards increment of pan protein and pY228 fraction. So, despite a tendency to a higher pY228 fraction, no significant change in p120 catenin and its pY228 fraction within 48 h have been proven.

Short-term BLM-treatment of murine PCLS serve as an in vitro model of early lung injury for investigating pathways before evolving manifest fibrotic changes as seen in previous studies [61]. BLM-treated PCLS of WT murine lung showed a significant decrease of p120 catenin pan protein after 48 h. Binding to E-Cadherin stabilizes AJ in the cell membrane, so loss of p120 catenin can also result in EMT [39,83], which is a common hallmark of PF [40] including COVID-19 [67]. Dissociation of lacking p120 catenin from E-Cadherin exposes its binding site for adapter protein 2 (AP-2) or the E3 ligase Hakai, leading to increased endocytosis or ubiquitination of E-Cadherin and therefore impaired cell adhesion [39]. Previous investigations showed a decrease of p120 catenin amount after short-term mechanical stress in murine AECs [84]. Reduction of p120 catenin during short-term injury with BLM could be a possible mechanism leading to this profibrotic state. The difference between injured human NCI-H441 cells and the PCLS of WT murine lung could be explained through different model properties. While human NCI-H441 cells represent a single cell type of AECs, PCLS are constituted of all resident cell types of lung tissue with possible intercellular interactions. Our results therefore indicate a more complex regulation and role of p120 catenin and its phosphorylation pY228.

The AECI-specific protein Cav-1 is known to control catenin levels in injury models via activation of transcriptional pathways, therefore regulating AJs and alveolar barrier integrity [85]. The human lung samples of acute COVID-19 showed a decrease in cav-1 protein abundance compared to the control group with similar proportional change in mRNA expression staying on a lower level in chronic course of COVID-19 and ILD group. Previous investigations have shown a decrease of cav-1 by percentage of stained area in human COVID-19 lung [24]. Important to mention, DAD occurring in COVID-19 leads to a damage of AECs, which results in smaller abundance of epithelial cell markers in tissue slices [22]. Due to our ROI definition, we also showed a lower abundance of the protein in the specific location of cav-1, indicating that it is even downregulated in cav-1 expressing cells. Cav-1 is known to be decreased in early lung injury models [86,87] and also in established PF [45,88,89]. Cav-1 knockout mice show several profibrotic changes in the lung with increased fibrillar deposition and, hematopoietic and endothelial progenitors and AECII hypertrophy as a potential result of altered regulation of gene transcription and cell differentiation [90], knockdown of cav-1 has been shown to regulate AJ proteins and cell migration: cav-1 knockdown downregulates E-Cadherin and AJ integrity, therefore impairing epithelial cell adhesion, facilitating cell migration and potentially increasing cytosolic abundance and above mentioned downstream signalling of p120 catenin or β-catenin [91,92]. In a spinal cord injury model, the protective effect of upregulating AJ proteins (including p120 catenin) is mediated by abundance of cav-1 [85]. Thus, reduction of cav-1 indicates an early involvement in fibrogenesis of COVID-19 impaired lungs. Since the endosomal cell entry of SARS-CoV-2 is dependent on cholesterol-rich lipid rafts which include caveolae, a potential colocalization and therefore interaction between cav-1 and SARS-CoV-2 is possible [93].

P2X7R is an ATP-gated cation channel in the cell membrane of different cell types, among others in the alveolar epithelium [65], included in several (patho)physiologic processes, i.e. inflammation, neurodegenerative diseases, neoplasia and fibrosis [64,94]. Extracellular ATP acts as a damage associated molecular pattern (DAMP) through activation and short-term upregulation of P2X7R, inducing further proinflammatory pathways [50,95].

P2X7R staining showed a decrement of protein abundance in the COVID-19 and ILD group. This could be explained through direct interaction with cav-1. A knockdown and knockout of cav-1 was described to downregulate transcription of P2X7R in pulmonary tissue, and P2X7R abundance regulates cav-1 vice versa. Additionally a direct interaction between both proteins serve to the recruitment of P2X7R into AEC caveolae [48,49,60,63,96]. Expression of P2X7R mRNA showed a trend towards up-regulation in COVID-19 chronic group. Another explanation for decreased P2X7R abundance, even though it acts as an alarm signal, could be decreased protein translation [97]. The interaction between P2X7R and cav-1 can be an explanation for the decrement of P2X7R in COVID-19.

Our investigations have several limitations. Early lung injury models using the single cell type (NCI-H441) and the 3D in vitro model of pulmonary tissue excluding humoral factors (murine PCLS) and post-mortem specimen of COVID-19 human lung serve different model properties and a different basis of pathogenesis, making it difficult to offer proper comparisons. Since NCI-H441 cell culture is lacking different, mutually interacting pulmonary cell types including (myo)fibroblasts and endothelial cells, generalizability of the findings to human or murine lung tissue is also limited. Nevertheless, common pathogenic processes have been described above. Additionally, instability of fluorescence can lead to more statistical scattering. Experimental conditions were kept rigorously equal to suit this issue.

Conclusion

To sum up the potential interactions between intercellular connections and associated caveolae-associated proteins we propose a model, shown in Figure 7. Further investigations on these interactions are necessary to fully elucidate the underlying mechanisms to find possible therapeutical approaches preventing fibrotic changes after early injury such as COVID-19 or other fibrotic diseases.

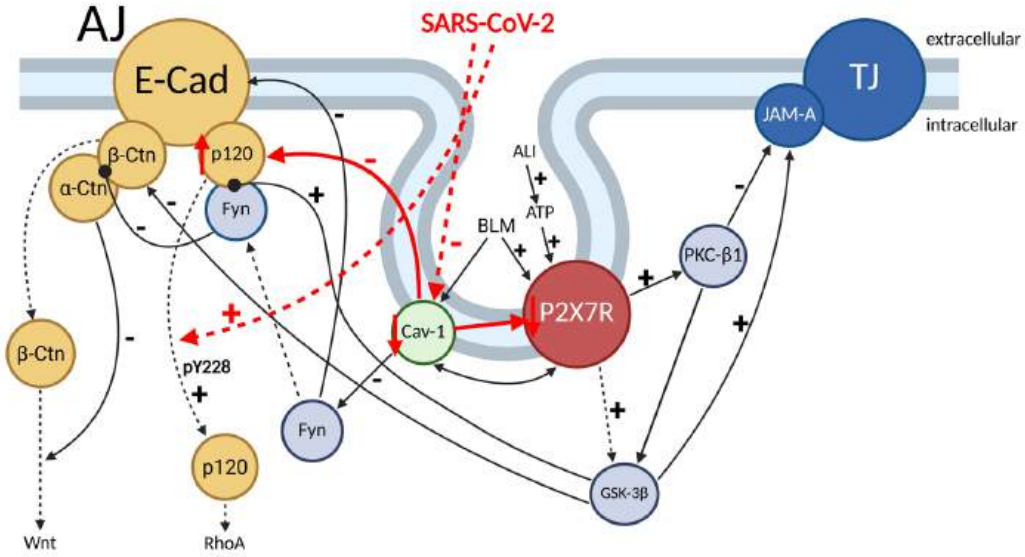

Figure 7: Potential interaction model between caveolae-associated proteins and intercellular connections

The caveolae-associated proteins cav-1 and P2X7R interact with each other and influence AJ and TJ proteins through direct as-sociation or signalling partners like kinases (PKC-β1, Fyn, GSK-3β) [98–105]. Acute lung injury (ALI), as in COVID-19, leadsto significant ATP-release, leading to activation of P2X7R [106–109]. Phosphorylations of β-Catenin or p120 catenin can leadto dissociation from the AJ, leading to activation of downstream signalling pathways (Wnt, Rho GTPases) [110,111]. Created inBioRender. Wiegner, J. (2025) https://BioRender.com/i61q937.

Figure 7: Publication-License

https://annexpublishers.com/articles/JCBH/Figure-7-Publication-License.pdf

Conflicts of Interest Statement

The authors declare no conflict of interest. The funders had no role in the design of the study; in the collection, analyses, or interpretation of data, in the writing of the manuscript, or in the decision to publish the results.

Acknowledgements

This work was funded by the Deutsche Forschungsgemeinschaft (DFG), BA 3899/4-2. The authors thank A. Neisser, M. Pinkert, D. Streichert, S. Bramke, N. Feind and K. Pehlke for their expert technical assistance and Dr. S. von Stillfried and Dr. M. Kühnel for their critical reading of the manuscript. Special thanks to Dr. Pablik for supporting us with sample collection. This work was funded by the research consortium NATON. The NATON project (grant number 01KX2121) is part of the National Network University Medicine (NUM), funded by the Federal Ministry of Education and Research (BMBF) in Germany. The National Network University Medicine is coordinated at the Charité - Universitätsmedizin Berlin and supervised by the German Aerospace Center (DLR Project Management Agency). The funders had no role in the study design, data collection and analysis, publication decision, or manuscript preparation. The human tissue samples used were provided by the Tumor and Normal Tissue Bank of the UCC Dresden and were used in accordance with the regulations of the tissue bank (and the approval of the Ethics Committee of the Technical University of Dresden).

Author Contributions

KB, JW and MK conceived the experiments; JW carried out the experiments, analysed the data and generated the figures; JW and KB were involved in data interpretation and writing the paper; all authors had final approval of the submitted and published versions.

Supplementary Information

https://www.annexpublishers.com/articles/JCBH/7102-Supplementary-Material.pdf

References

1. Bagnato G, Harari S (2015) Cellular interactions in the pathogenesis of interstitial lung diseases. Eur Respir Rev 24: 102–114.

2. Crouch E (1990) Pathobiology of pulmonary fibrosis. Am J Physiol 259 (4 Pt 1): L159-84.

3. Katzenstein AL, Myers JL (1998) Idiopathic pulmonary fibrosis: clinical relevance of pathologic classification. Am J Respir Crit Care Med 157: 1301–115.

4. Selman M, King TE, Pardo A (2001) Idiopathic pulmonary fibrosis: prevailing and evolving hypotheses about its pathogenesis and implications for therapy. Ann Intern Med 134: 136–151.

5. Thannickal VJ, Toews GB, White ES, Lynch JP, Martinez FJ (2004) Mechanisms of pulmonary fibrosis. Annu Rev Med 55: 395–417.

6. Visscher DW, Myers JL (2006) Histologic spectrum of idiopathic interstitial pneumonias. Proc Am Thorac Soc 3: 322–329.

7. Bösmüller H, Matter M, Fend F, Tzankov A (2021) The pulmonary pathology of COVID-19. Virchows Arch 478: 137–150.

8. Flaifel A, Kwok B, Ko J, Chang S, Smith D, et al. (2022) Pulmonary Pathology of End-Stage COVID-19 Disease in Explanted Lungs and Outcomes After Lung Transplantation. Am J Clin Pathol 157: 908–926.

9. Gorbalenya AE, Baker SC, Baric RS, Groot RJ de, Drosten C, et al. (2020) Severe acute respiratory syndrome-related coronavirus: The species and its viruses – a statement of the Coronavirus Study Group.

10. Nurchis MC, Pascucci D, Sapienza M, Villani L, D'Ambrosio F, et al. (2020) Impact of the Burden of COVID-19 in Italy: Results of Disability-Adjusted Life Years (DALYs) and Productivity Loss. Int J Environ Res Public Health 17.

11. Matthay MA, Zemans RL, Zimmerman GA, Arabi YM, Beitler JR, et al. (2019) Acute respiratory distress syndrome. Nat Rev Dis Primers 5: 18.

12. Tojo K, Yamamoto N, Tamada N, Mihara T, Abe M, et al. (2023) Early alveolar epithelial cell necrosis is a potential driver of COVID-19-induced acute respiratory distress syndrome. iScience 26: 105748.

13. Azagew AW, Beko ZW, Ferede YM, Mekonnen HS, Abate HK, et al. (2023) Global prevalence of COVID-19-induced acute respiratory distress syndrome: systematic review and meta-analysis. Syst Rev 12: 212.

14. Li X, Shen C, Wang L, Majumder S, Zhang D, et al. (2021) Pulmonary fibrosis and its related factors in discharged patients with new corona virus pneumonia: a cohort study. Respir Res 22: 203.

15. Groff D, Sun A, Ssentongo AE, Ba DM, Parsons N, et al. (2021) Short-term and Long-term Rates of Postacute Sequelae of SARS-CoV-2 Infection: A Systematic Review. JAMA Netw Open 4: e2128568.

16. Yao X-H, Luo T, Shi Y, He Z-C, Tang R, et al. (2021) A cohort autopsy study defines COVID-19 systemic pathogenesis. Cell Res 31: 836–846.

17. Tian S, Xiong Y, Liu H, Niu L, Guo J, et al. (2020) Pathological study of the 2019 novel coronavirus disease (COVID-19) through postmortem core biopsies. Mod Pathol 33: 1007–1014.

18. Xu Z, Shi L, Wang Y, Zhang J, Huang L, et al. (2020) Pathological findings of COVID-19 associated with acute respiratory distress syndrome. Lancet Respir Med 8: 420–422.

19. Kramann R, DiRocco DP, Humphreys BD (2013) Understanding the origin, activation and regulation of matrix-producing myofibroblasts for treatment of fibrotic disease. J. Pathol. 231: 273–289.

20. Saha P, Talwar P (2024) Idiopathic pulmonary fibrosis (IPF): disease pathophysiology, targets, and potential therapeutic interventions. Molecular and cellular biochemistry 479: 2181–2194.

21. Kajdaniuk D, Marek B, Borgiel-Marek H, Kos-Kudła B (2013) Transforming growth factor β1 (TGFβ1) in physiology and pathology. Endokrynol Pol 64: 384–396.

22. D'Agnillo F, Walters K-A, Xiao Y, Sheng Z-M, Scherler K, et al. (2021) Lung epithelial and endothelial damage, loss of tissue repair, inhibition of fibrinolysis, and cellular senescence in fatal COVID-19. Sci Transl Med 13: eabj7790.

23. Broekelmann TJ, Limper AH, Colby TV, McDonald JA (1991) Transforming growth factor beta 1 is present at sites of extracellular matrix gene expression in human pulmonary fibrosis. Proc Natl Acad Sci U S A 88: 6642–6646.

24. Vaz de Paula CB, Nagashima S, Liberalesso V, Collete M, da Silva FPG, et al. (2021) COVID-19: Immunohistochemical Analysis of TGF-β Signaling Pathways in Pulmonary Fibrosis. Int J Mol Sci 23.

25. Kasper M, Haroske G (1996) Alterations in the alveolar epithelium after injury leading to pulmonary fibrosis. Histol Histopathol 11: 463–483.

26. Brune K, Frank J, Schwingshackl A, Finigan J, Sidhaye VK (2015) Pulmonary epithelial barrier function: some new players and mechanisms. American Journal of Physiology-Lung Cellular and Molecular Physiology 308: L731-45.

27. Koval M (2013) Claudin heterogeneity and control of lung tight junctions. Annu Rev Physiol 75: 551–567.

28. Crapo JD, Barry BE, Gehr P, Bachofen M, Weibel ER (1982) Cell number and cell characteristics of the normal human lung. Am Rev Respir Dis 126: 332–337.

29. Garcia MA, Nelson WJ, Chavez N (2018) Cell-Cell Junctions Organize Structural and Signaling Networks. Cold Spring Harb Perspect Biol 10: a029181.

30. Shin K, Fogg VC, Margolis B (2006) Tight junctions and cell polarity. Annu Rev Cell Dev Biol 22 (Volume 22, 2006): 207–235.

31. Takeichi M (1991) Cadherin cell adhesion receptors as a morphogenetic regulator. Science 251: 1451–1455.

32. Stappert J, Kemler R (1999) The Cadherin Superfamily In The adhesive interaction of cells, Garrod DR (ed), JAI Press, Stamford, Conn.; 27–63 (Advances in Molecular and Cell Biology; vol 28).

33. Nagafuchi A, Takeichi M (1988) Cell binding function of E-cadherin is regulated by the cytoplasmic domain. EMBO J 7: 3679–3684.

34. Ishiyama N, Lee S-H, Liu S, Li G-Y, Smith MJ, et al. (2010) Dynamic and static interactions between p120 catenin and E--cadherin regulate the stability of cell-cell adhesion. Cell 141: 117–128.

35. Ozawa M, Baribault H, Kemler R (1989) The cytoplasmic domain of the cell adhesion molecule uvomorulin associates with three independent proteins structurally related in different species. EMBO J 8: 1711–1717.

36. Reynolds AB, Daniel J, McCrea PD, Wheelock MJ, Wu J, et al. (1994) Identification of a new catenin: the tyrosine kinase substrate p120cas associates with E-cadherin complexes. Mol Cell Biol 14: 8333–8342.

37. Reynolds AB, Roczniak-Ferguson A (2004) Emerging roles for p120-catenin in cell adhesion and cancer. Oncogene 23: 7947–7956.

38. Anastasiadis PZ, Reynolds AB (2001) Regulation of Rho GTPases by p120-catenin. Curr Opin Cell Biol 13: 604–610.

39. Kourtidis A, Ngok SP, Anastasiadis PZ (2013) p120 catenin: an essential regulator of cadherin stability, adhesion-induced signaling, and cancer progression. Prog Mol Biol Transl Sci 116: 409–432.

40. Lamouille S, Xu J, Derynck R (2014) Molecular mechanisms of epithelial-mesenchymal transition. Nat Rev Mol Cell Biol 15: 178–196.

41. Razani B, Woodman SE, Lisanti MP (2002) Caveolae: from cell biology to animal physiology. Pharmacol Rev 54: 431–467.

42. Koleske AJ, Baltimore D, Lisanti MP (1995) Reduction of caveolin and caveolae in oncogenically transformed cells. Proc Natl Acad Sci U S A 92: 1381–1385.

43. Gabazza EC, Kasper M, Ohta K, Keane M, D'Alessandro-Gabazza C, et al. (2004) Decreased expression of aquaporin-5 in bleomycin-induced lung fibrosis in the mouse. Pathol Int 54: 774–780.

44. Lamaze C, Tardif N, Dewulf M, Vassilopoulos S, Blouin CM (2017) The caveolae dress code: structure and signaling. Curr Opin Cell Biol 47: 117–125.

45. Del Galdo F, Sotgia F, Almeida CJ de, Jasmin J-F, Musick M, et al. (2008) Decreased expression of caveolin 1 in patients with systemic sclerosis: crucial role in the pathogenesis of tissue fibrosis. Arthritis Rheum 58: 2854–2865.

46. Xu S, Xue X, You K, Fu J (2016) Caveolin-1 regulates the expression of tight junction proteins during hyperoxia-induced pulmonary epithelial barrier breakdown. Respir Res 17: 50.

47. Lu Z, Ghosh S, Wang Z, Hunter T (2003) Downregulation of caveolin-1 function by EGF leads to the loss of E-cadherin, increased transcriptional activity of beta-catenin, and enhanced tumor cell invasion. Cancer Cell 4: 499–515.

48. Barth K, Weinhold K, Guenther A, Young MT, Schnittler H, et al. (2007) Caveolin-1 influences P2X7 receptor expression and localization in mouse lung alveolar epithelial cells. FEBS J 274: 3021–3033.

49. Barth K, Weinhold K, Guenther A, Linge A, Gereke M, et al. (2008) Characterization of the molecular interaction between caveolin-1 and the P2X receptors 4 and 7 in E10 mouse lung alveolar epithelial cells. Int J Biochem Cell Biol 40: 2230–2239.

50. Gentile D, Natale M, Lazzerini PE, Capecchi PL, Laghi-Pasini F (2015) The role of P2X7 receptors in tissue fibrosis: a brief review. Purinergic Signal 11: 435–440.

51. Adinolfi E, Giuliani AL, Marchi E de, Pegoraro A, Orioli E, et al. (2018) The P2X7 receptor: A main player in inflammation. Biochem Pharmacol 151: 234–244.

52. Travis WD, Costabel U, Hansell DM, King TE, Lynch DA, et al. (2013) An official American Thoracic Society/European Respiratory Society statement: Update of the international multidisciplinary classification of the idiopathic interstitial pneumonias. Am J Respir Crit Care Med 188: 733–748.

53. Salomon JJ, Muchitsch VE, Gausterer JC, Schwagerus E, Huwer H, et al. (2014) The cell line NCl-H441 is a useful in vitro model for transport studies of human distal lung epithelial barrier. Mol Pharm 11: 995–1006.

54. Kielgast F, Schmidt H, Braubach P, Winkelmann VE, Thompson KE, et al. (2016) Glucocorticoids Regulate Tight Junction Permeability of Lung Epithelia by Modulating Claudin 8. Am J Respir Cell Mol Biol 54: 707–717.

55. Hermanns MI, Unger RE, Kehe K, Peters K, Kirkpatrick CJ (2004) Lung epithelial cell lines in coculture with human pulmonary microvascular endothelial cells: development of an alveolo-capillary barrier in vitro. Lab Invest 84: 736–752.

56. Neuhaus W, Samwer F, Kunzmann S, Muellenbach RM, Wirth M, et al. (2012) Lung endothelial cells strengthen, but brain endothelial cells weaken barrier properties of a human alveolar epithelium cell culture model. Differentiation 84: 294–304.

57. Weinhold K (2010) Molekulare und biochemische Charakterisierung der purinergen Rezeptoren P2X4 und P2X7 im Alveolarepithel der Lunge.

58. Held HD, Martin C, Uhlig S (1999) Characterization of airway and vascular responses in murine lungs. Br J Pharmacol 126: 1191–1199.

59. Ebeling G, Bläsche R, Hofmann F, Augstein A, Kasper M, et al. (2014) Effect of P2X7 receptor knockout on AQP-5 expression of type I alveolar epithelial cells. PLoS One 9: e100282.

60. Hofmann F, Bläsche R, Kasper M, Barth K (2015) A co-culture system with an organotypic lung slice and an immortal alveolar macrophage cell line to quantify silica-induced inflammation. PLoS One 10: e0117056.

61. Barth K, Bläsche R, Kasper M (2006) Lack of evidence for caveolin-1 and CD147 interaction before and after bleomycin-induced lung injury. Histochem Cell Biol 126: 563–573.

62. Shihan MH, Novo SG, Le Marchand SJ, Wang Y, Duncan MK (2021) A simple method for quantitating confocal fluorescent images. Biochem Biophys Rep 25: 100916.

63. Barth K, Kasper M (2009) Membrane compartments and purinergic signalling: occurrence and function of P2X receptors in lung. FEBS J 276: 341–353.

64. Burnstock G (2006) Pathophysiology and therapeutic potential of purinergic signaling. Pharmacol Rev 58: 58–86.

65. Chen Z, Jin N, Narasaraju T, Chen J, McFarland LR, et al. (2004) Identification of two novel markers for alveolar epithelial type I and II cells. Biochem Biophys Res Commun 319: 774–780.

66. Li Z, Wermuth PJ, Benn BS, Lisanti MP, Jimenez SA (2013) Caveolin-1 deficiency induces spontaneous endothelial-to-mesenchymal transition in murine pulmonary endothelial cells in vitro. Am J Pathol 182: 325–331.

67. Rendeiro AF, Ravichandran H, Bram Y, Chandar V, Kim J, et al. (2021) The spatial landscape of lung pathology during COVID-19 progression. Nature 593: 564–569.

68. Valdebenito S, Bessis S, Annane D, La Lorin de Grandmaison G, Cramer-Bordé E, et al. (2021) COVID-19 Lung Pathogenesis in SARS-CoV-2 Autopsy Cases. Front Immunol 12: 735922.

69. Martinez FJ, Collard HR, Pardo A, Raghu G, Richeldi L, et al. (2017) Idiopathic pulmonary fibrosis. Nat Rev Dis Primers 3: 17074.

70. Willis BC, Borok Z (2007) TGF-beta-induced EMT: mechanisms and implications for fibrotic lung disease. American Journal of Physiology-Lung Cellular and Molecular Physiology 293: L525-34.

71. Ackermann M, Verleden SE, Kuehnel M, Haverich A, Welte T, et al. (2020) Pulmonary Vascular Endothelialitis, Thrombosis, and Angiogenesis in Covid-19. N Engl J Med 383: 120–128.

72. Takeichi M (2014) Dynamic contacts: rearranging adherens junctions to drive epithelial remodelling. Nat Rev Mol Cell Biol 15: 397–410.

73. Davis MA, Ireton RC, Reynolds AB (2003) A core function for p120-catenin in cadherin turnover. J Cell Biol 163: 525–534.

74. Ireton RC, Davis MA, van Hengel J, Mariner DJ, Barnes K, et al. (2002) A novel role for p120 catenin in E-cadherin function. J Cell Biol 159: 465–476.

75. Zhang Y, Jiao H, Wu Y, Sun X (2019) P120-catenin regulates pulmonary fibrosis and TGF-β induced lung fibroblast differentiation. Life Sci 230: 35–44.

76. Ding X, Wang X, Lu S, Gao X, Ju S (2019) P120-Catenin And Its Phosphorylation On Tyr228 Inhibits Proliferation And Invasion In Colon Adenocarcinoma Cells. Onco Targets Ther 12: 10213–10225.

77. Castaño J, Solanas G, Casagolda D, Raurell I, Villagrasa P, et al. (2007) Specific phosphorylation of p120-catenin regulatory domain differently modulates its binding to RhoA. Mol Cell Biol 27: 1745–1757.

78. Huveldt D, Lewis-Tuffin LJ, Carlson BL, Schroeder MA, Rodriguez F, et al. (2013) Targeting Src family kinases inhibits bevacizumab-induced glioma cell invasion. PLoS One 8: e56505.

79. Kuroda S, Fukata M, Nakagawa M, Fujii K, Nakamura T, et al. (1998) Role of IQGAP1, a target of the small GTPases Cdc42 and Rac1, in regulation of E-cadherin- mediated cell-cell adhesion. Science 281: 832–835.

80. Bhowmick NA, Ghiassi M, Bakin A, Aakre M, Lundquist CA, et al. (2001) Transforming growth factor-beta1 mediates epithelial to mesenchymal transdifferentiation through a RhoA-dependent mechanism. Mol Biol Cell 12: 27–36.

81. Watson RA, La Peña H de, Tsakok MT, Joseph J, Stoneham S, et al. (2018) Development of a best-practice clinical guideline for the use of bleomycin in the treatment of germ cell tumours in the UK. Br J Cancer 119: 1044–1051.

82. Della Latta V, Cecchettini A, Del Ry S, Morales MA (2015) Bleomycin in the setting of lung fibrosis induction: From biological mechanisms to counteractions. Pharmacol Res 97: 122–130.

83. Davis MA, Reynolds AB (2006) Blocked acinar development, E-cadherin reduction, and intraepithelial neoplasia upon ablation of p120-catenin in the mouse salivary gland. Dev Cell 10: 21–31.

84. Dai C, Dai G, Sun Y, Wang Y (2013) Loss of p120 catenin aggravates alveolar edema of ventilation induced lung injury. Chin Med J (Engl) 126: 2918–2922.

85. Ye L-B, Yu X-C, Xia Q-H, Yang Y, Chen D-Q, et al. (2016) Regulation of Caveolin-1 and Junction Proteins by bFGF Contributes to the Integrity of Blood-Spinal Cord Barrier and Functional Recovery. Neurotherapeutics 13: 844–858.

86. Menzel V, Ziegler M, Hante N, Sake JA, Santos-Martinez MJ, et al. (2022) Fyn-kinase and caveolin-1 in the alveolar epithelial junctional adherence complex contribute to the early stages of pulmonary fibrosis. Eur J Pharm Sci 175: 106236.

87. Koslowski R, Barth K, Augstein A, Tschernig T, Bargsten G, et al. (2004) A new rat type I-like alveolar epithelial cell line R3/1: bleomycin effects on caveolin expression. Histochem Cell Biol 121: 509–519.

88. Kasper M, Reimann T, Hempel U, Wenzel KW, Bierhaus A, et al. (1998) Loss of caveolin expression in type I pneumocytes as an indicator of subcellular alterations during lung fibrogenesis. Histochem Cell Biol 109: 41–48.

89. Shetty S, Idell S (2023) Caveolin-1-Related Intervention for Fibrotic Lung Diseases. Cells 12.

90. Drab M, Verkade P, Elger M, Kasper M, Lohn M, et al. (2001) Loss of caveolae, vascular dysfunction, and pulmonary defects in caveolin-1 gene-disrupted mice. Science 293: 2449–2452.

91. Song Y, Xue L, Du S, Sun M, Hu J, et al. (2012) Caveolin-1 knockdown is associated with the metastasis and proliferation of

human lung cancer cell line NCI-H460. Biomed Pharmacother 66: 439–447.

92. Galbiati F, Volonte D, Brown AM, Weinstein DE, Ben-Ze'ev A, et al. (2000) Caveolin-1 expression inhibits Wnt/beta-catenin/Lef-1 signaling by recruiting beta-catenin to caveolae membrane domains. J Biol Chem 275: 23368–23377.

93. Li X, Zhu W, Fan M, Zhang J, Peng Y, et al. (2021) Dependence of SARS-CoV-2 infection on cholesterol-rich lipid raft and endosomal acidification. Comput Struct Biotechnol J 19: 1933–1943.

94. Riteau N, Gasse P, Fauconnier L, Gombault A, Couegnat M, et al. (2010) Extracellular ATP is a danger signal activating P2X7 receptor in lung inflammation and fibrosis. Am J Respir Crit Care Med 182: 774–783.

95. Bläsche R, Ebeling G, Perike S, Weinhold K, Kasper M, et al. (2012) Activation of P2X7R and downstream effects in bleomycin treated lung epithelial cells. Int J Biochem Cell Biol 44: 514–524.

96. Weinhold K, Krause-Buchholz U, Rödel G, Kasper M, Barth K (2010) Interaction and interrelation of P2X7 and P2X4 receptor complexes in mouse lung epithelial cells. Cell Mol Life Sci 67: 2631–2642.

97. Ghosh A, Shcherbik N (2020) Effects of Oxidative Stress on Protein Translation: Implications for Cardiovascular Diseases. Int J Mol Sci 21: 2661.

98. Barth K, Bläsche R, Neißer A, Bramke S, Frank JA, et al. (2016) P2X7R-dependent regulation of glycogen synthase kinase 3β and claudin-18 in alveolar epithelial type I cells of mice lung. Histochem Cell Biol 146: 757–768.

99. Wesslau K-P, Stein A, Kasper M, Barth K (2019) P2X7 Receptor Indirectly Regulates the JAM-A Protein Content via Modulation of GSK-3β. Int J Mol Sci 20.

100. Lickert H, Bauer A, Kemler R, Stappert J (2000) Casein kinase II phosphorylation of E-cadherin increases E-cadherin/beta-catenin interaction and strengthens cell-cell adhesion. J Biol Chem 275: 5090–5095.

101. Liu C, Li Y, Semenov M, Han C, Baeg G-H, et al. (2002) Control of β-Catenin Phosphorylation/Degradation by a Dual-Kinase Mechanism. Cell 108: 837–847.

102. Piedra J, Miravet S, Castaño J, Pálmer HG, Heisterkamp N, et al. (2003) p120 Catenin-associated Fer and Fyn tyrosine kinases regulate beta-catenin Tyr-142 phosphorylation and beta-catenin-alpha-catenin Interaction. Mol Cell Biol 23: 2287–2297.

103. Kim AN, Jeon W-K, Lim K-H, Lee H-Y, Kim WJ, et al. (2011) Fyn mediates transforming growth factor-beta1-induced down-regulation of E-cadherin in human A549 lung cancer cells. Biochem Biophys Res Commun 407: 181–184.

104. Song KS, Li S, Okamoto T, Quilliam LA, Sargiacomo M, et al. (1996) Co-purification and direct interaction of Ras with caveolin, an integral membrane protein of caveolae microdomains. Detergent-free purification of caveolae microdomains. J Biol Chem 271: 9690–9697.

105. Li S, Couet J, Lisanti MP (1996) Src tyrosine kinases, Galpha subunits, and H-Ras share a common membrane-anchored scaffolding protein, caveolin. Caveolin binding negatively regulates the auto-activation of Src tyrosine kinases. J Biol Chem 271: 29182–29190.

106. Cicko S, Köhler TC, Ayata CK, Müller T, Ehrat N, et al. (2018) Extracellular ATP is a danger signal activating P2X7 receptor in a LPS mediated inflammation (ARDS/ALI). Oncotarget 9: 30635–30648.

107. Burnstock G (2013) Purinergic signalling: pathophysiology and therapeutic potential. Keio J Med 62: 63–73.

108. Hasan D, Shono A, van Kalken CK, van der Spek PJ, Krenning EP, et al. (2022) A novel definition and treatment of hyper-inflammation in COVID-19 based on purinergic signalling. Purinergic Signal 18: 13–59.

109. Pacheco PAF, Faria RX (2021) The potential involvement of P2X7 receptor in COVID-19 pathogenesis: A new therapeutic target? Scand J Immunol 93: e12960.

110. Huber AH, Nelson WJ, Weis WI (1997) Three-dimensional structure of the armadillo repeat region of beta-catenin. Cell 90: 871–882.

111. Choi SH, Estarás C, Moresco JJ, Yates JR, Jones KA (2013) α-Catenin interacts with APC to regulate β-catenin proteolysis and transcriptional repression of Wnt target genes. Genes Dev 27: 2473–2488.